

Enhanced Organocatalytic Processes through an Engineered Acid-Base Site Bifunctional Pore in a Zirconium Metal-Organic Framework

José María Moreno,^[a, b] Rodrigo Gil-San-Millan,^[a] Rubén Mas-Ballesté,^[a, c] José Alemán,^{*,[b, c]} and Ana E. Platero-Prats^{*,[a, d]}

This work introduces a robust acid-base catalytic system based on the zirconium-based metal-organic framework (Zr-MOF) MOF-808, selected for its open structure, high stability, and low presence of structural defects compared to other Zr-MOFs. Four bifunctional benzoate ligands bearing free carboxylic acid (-COOH) and nitrogen-containing groups were introduced into the MOF-808 using solvent-assisted ligand exchange methods. Unlike other materials, the acid and base sites in the bifunctional MOF-808 materials are situated in the same capping ligand, leading to a bifunctional behavior between the two

neighboring sites. The system was tested for Knoevenagel condensation and deacetylation-Knoevenagel tandem reactions, demonstrating high catalytic activity and excellent yields. Additionally, computational modeling provided insights into the catalytic mechanism and the role of the acid-base sites. The study provides a better understanding of the unique behavior of the bifunctional MOF-808 catalyst and offers prospects for designing new and efficient catalytic systems for organo-catalysis.

1. Introduction

Chemical sectors aim to enhance synthetic processes' efficiency while reducing the use of raw materials, energy, and waste generation, resulting in a decreased environmental footprint. To accomplish this objective, there is an increasing need for novel catalysts that can provide higher activity, selectivity, and recyclability to produce chemical compounds. The Knoevenagel condensation reaction is an example of a catalyzed chemical reaction that is widely used in the production of pharmaceuticals, cosmetics, and fine chemicals. This reaction is accelerated in the presence of a basic catalyst, and porous materials are being explored as promising catalytic platforms as they provide easy access to the active sites within the pore systems.^[1]

Metal-organic frameworks (MOFs) are part of the toolbox of porous heterogeneous catalysts and their research, development, and implementation have increased over the last three decades.^[2] MOFs are crystalline, highly porous materials obtained by the self-assembly of metal nodes (ions or clusters, also known as secondary building units, SBUs) with multitopic organic ligands through coordination bonds. One of the key features of MOFs is that they can be tailored to meet the requirements of a specific reaction, as a virtually infinite number of metal and organic components can be strategically assembled into the framework. In this manner, topology, pore size, and chemical composition can be rationally designed to achieve confinement effects in the functionalised pores, which contain catalytic sites operating with high selectivity.^[3] The active site of MOF-based catalysts can be located in the SBU, in the organic ligand, or in an introduced specie inside the pore (e.g., clusters, nanoparticles).^[4] When the catalytic site is located in the ligand, it can be already present on the organic molecule prior to MOF synthesis, or it can be post-synthetically introduced after MOF synthesis. In some cases, the bridging and non-bridging (i.e., pendant) ligands initially coordinated to the SBU, can be replaced with new ligands containing the desired functionality, in a process known as Solvent-Assisted Ligand Exchange (SALE).^[5] The SALE method permits the production of finely restricted environments for catalyzing chemical reactions with remarkable selectivity.

The unique characteristics of MOFs described above enable the development of a bifunctional system with two distinct functionalities located in close proximity to each other, such an acid and a basic site. This prevents any harmful 'auto-quenching' event and generates synergistic effects in catalysis,^[6] including tandem or cascade reactions.^[7] Acid-base bifunctional MOF-based catalysts have been investigated for the Knoevena-

[a] J. M. Moreno, R. Gil-San-Millan, R. Mas-Ballesté, A. E. Platero-Prats
Departamento de Química Inorgánica, Facultad de Ciencias, Universidad Autónoma de Madrid, Campus de Cantoblanco, 28049 Madrid, Spain
E-mail: ana.platero@uam.es

[b] J. M. Moreno, J. Alemán
Departamento de Química Orgánica, Facultad de Ciencias, Universidad Autónoma de Madrid, Campus de Cantoblanco, 28049 Madrid, Spain
E-mail: jose.aleman@uam.es

[c] R. Mas-Ballesté, J. Alemán
Institute for Advanced Research in Chemical Sciences (IAdChem), Facultad de Ciencias, Universidad Autónoma de Madrid, Campus de Cantoblanco, 28049 Madrid, Spain.

[d] A. E. Platero-Prats
Condensed Matter Physics Center (IFIMAC), Facultad de Ciencias, Universidad Autónoma de Madrid, Campus de Cantoblanco, 28049 Madrid, Spain.

Supporting information for this article is available on the WWW under <https://doi.org/10.1002/cctc.202400676>

© 2024 The Authors. ChemCatChem published by Wiley-VCH GmbH. This is an open access article under the terms of the Creative Commons Attribution License, which permits use, distribution and reproduction in any medium, provided the original work is properly cited.

gel condensation as well as the one-pot tandem deacetylation-Knoevenagel reaction.^[8] The acid and base functionalities can be positioned in different sites within the network, such as (i) on the metallic SBU (Lewis acid site) and the ligand (basic site),^[8a-e] or (ii) in two different ligands (bridging or pendant) situated in close proximity.^[8f,g] While several stable zirconium-based MOFs (Zr-MOFs), including UiO-66 or UiO-67, have been investigated for Knoevenagel condensation,^[9,8h] their acidic catalytic activity has predominantly relied on the metallic centers (Zr(IV)) for activating the electrophilic center (aldehyde). Consequently, these reactions typically needed high catalyst loadings (see benchmark Table S2 for similar Zr-MOF systems).

In this work, a robust acid-base catalytic system based on a zirconium MOF is presented. The MOF-808 (Figure 1) was chosen due to its open structure, high stability and lower presence of structural defects compared to other Zr-MOFs. Four different bifunctionalized benzoate ligands bearing free carboxylic acid (-COOH) and nitrogen-containing groups were introduced into the MOF-808 via a solvent-assisted ligand exchange (SALE) method. Unlike other materials where the functionalities are located on the SBU or the organic spacer, the acid and base sites in the MOF-808 are in the same capping ligand, allowing for a bifunctional behavior between the two neighboring sites. This innovative approach resulted in a highly robust system that was tested for the Knoevenagel reaction and the deacetylation-Knoevenagel tandem reaction, demonstrating its immense potential for catalysis. Furthermore, computational modelling was employed to gain insights into the catalytic mechanism of the MOF-808 system. The results of the modelling study provided a detailed understanding of the reaction pathway and the role of the acid-base sites in the catalytic activity of the system. This combined experimental and computational approach sheds light on the unique bifunctional behavior of the MOF-808 catalyst and offers opportunities for the rational design of new and efficient catalytic systems for enhanced organocatalysis.

2. Results and Discussion

2.1. Syntheses and Characterization

MOF-808 was selected as a suitable MOF platform, synthesized following a reported protocol,^[10] and then modified by solvent-assisted ligand exchange (SALE) method.^[11] In this manner, four MOFs were obtained with different bifunctional benzoate N-containing ligands with increasing basicity: pyridine-4-carboxylic acid (**MOF-808-PyC**), pyridine-3,5-dicarboxylic acid (**MOF-808-PyDC**), 4-aminobenzoic acid (**MOF-808-4AB**) and 5-aminoisophthalic acid (**MOF-808-5AIP**) (Figure 2a). An optimal loading of the bifunctional ligands within MOF-808 was achieved using a ligand to MOF molar ratio of 10, in N,N-dimethylformamide (DMF) at 85 °C for 24 h (see Supporting Information, S.I.). The obtained materials were digested under acidic conditions and analyzed by ¹H NMR (Figure S5) to determine the chemical composition of the MOF-808 based frameworks (Table 1). The results revealed that all bifunctional benzoate ligands were successfully incorporated, obtaining a higher loading for the pyridine ligands (2.8–2.9 ligands per Zr₆ cluster) compared to amino ligands (1.5–1.6 ligands per Zr₆ cluster). This is attributed to the lower *pK_a* values of pyridine ligands compared to the amine counterparts, which favors the coordination of the carboxylates with the highly acidic Zr(IV) centers.^[12] In all cases, some remaining formate ligands are coordinated to the Zr₆O₄(OH)₄ cluster. It is worth mentioning that pyridine-3,5-dicarboxylic acid (PyDC) and 5-aminoisophthalic acid (5AIP) have been previously introduced, pre-synthetically, in MOF-808 yielding defective systems with much lower amount of functionalized ligand (< 10 mol%).^[13] On the other hand, our approach preserves the structural integrity of the MOF and maximize the loading of bifunctional ligands.

X-ray diffraction (PXRD) data were collected on the modified materials, demonstrating the occurrence of the Bragg reflections corresponding to MOF-808 in all cases, as well as the

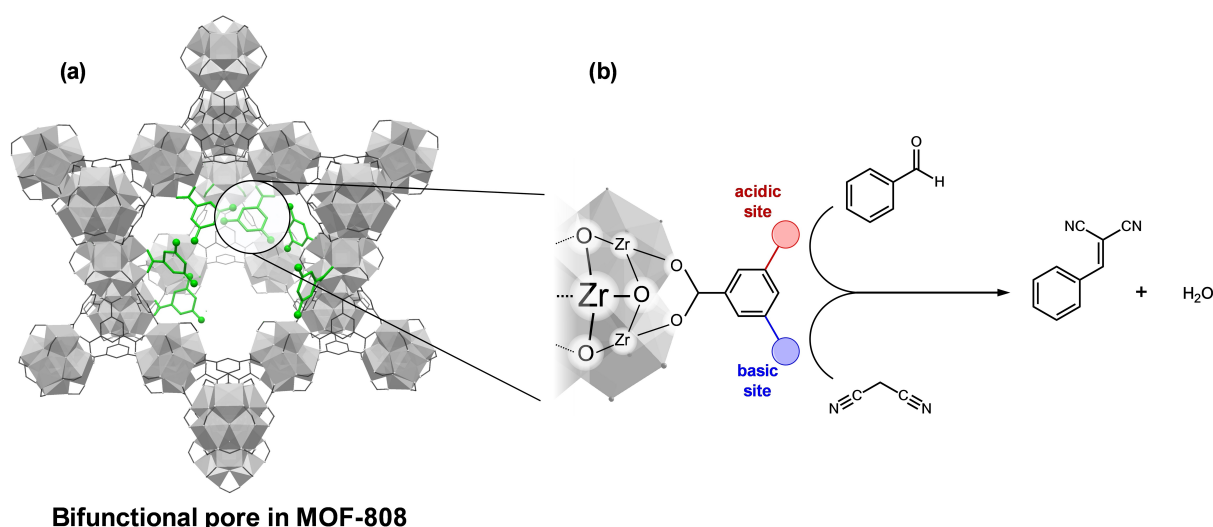


Figure 1. (a) MOF 3D structure for MOF-808 containing bifunctional, pendant ligands (green). (b) Acid-base bifunctional catalysis of the Knoevenagel condensation within a functionalized MOF-808. H atoms in MOF cluster are omitted for clarity.

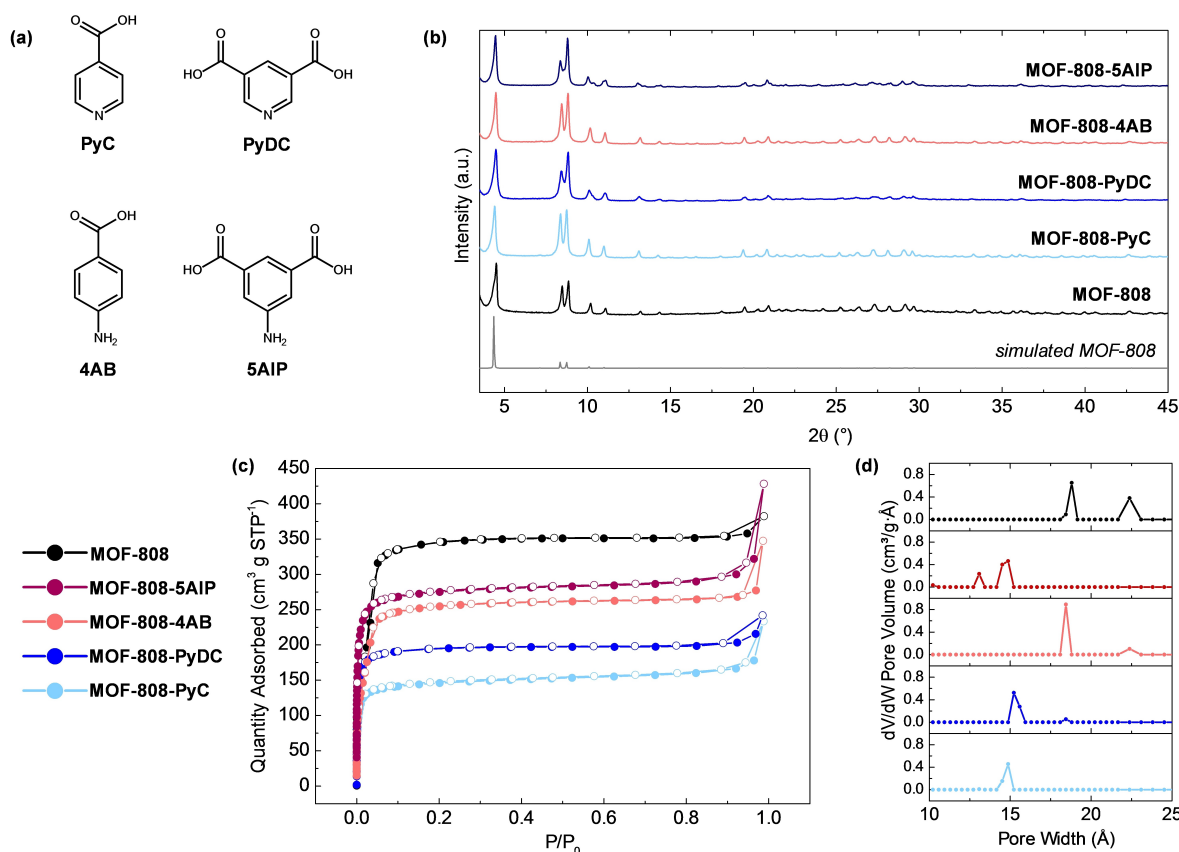


Figure 2. Structural characterization of post-synthetically modified MOF-808 materials. (a) Benzoate ligands used in this work for the functionalization of MOF-808, namely pyridine-4-carboxylic acid (PyC), pyridine-3,5-dicarboxylic acid (PyDC), 4-aminobenzoic acid (4AB) and 5-aminoisophthalic acid (5AIP). (b) Powder X-ray diffractograms, (c) N₂ adsorption isotherms (empty circles denote the desorption branch), and (d) density functional theory (DFT) analyses of pore size distribution for MOF-808 based materials.

Table 1. Characterization and catalytic results in the Knoevenagel condensation between benzaldehyde and malononitrile for SALE-modified MOF-808 materials.

Materials	Chemical formula (¹ H NMR) ^a	BET surface area [m ² /g]	Yield [%] ^b
blank	–	–	0
MOF-808	Zr ₆ O ₄ (OH) ₄ (BTC) ₂ (HCOO) ₆	1248 ± 20	20
MOF-808-5AIP	Zr ₆ O ₄ (OH) ₄ (BTC) ₂ (5AIP) _{1.5} (HCOO) ₂ (H ₂ O) _{2.5} (OH) _{2.5}	1076 ± 5	100
MOF-808-4AB	Zr ₆ O ₄ (OH) ₄ (BTC) ₂ (4AB) _{1.6} (HCOO) _{3.4} (H ₂ O)(OH)	969 ± 22	45
MOF-808-PyDC	Zr ₆ O ₄ (OH) ₄ (BTC) ₂ (PyDC) _{2.9} (HCOO) _{2.3} (H ₂ O) _{0.8} (OH) _{0.8}	774 ± 8	74
MOF-808-PyC	Zr ₆ O ₄ (OH) ₄ (BTC) ₂ (PyC) _{2.8} (HCOO) _{2.3} (H ₂ O) _{0.9} (OH) _{0.9}	566 ± 3	11

^a) Normalized to 2 BTC. BTC: benzene-1,3,5-tricarboxylate, 5AIP: 5-aminoisophthalate, 4AB: 4-Aminobenzoate, PyDC: pyridine-3,5-dicarboxylate, PyC: 4-pyridinecarboxylate; ^b) Reactions conditions: benzaldehyde (0.27 mmol), malononitrile (0.28 mmol), 0.5 mL acetonitrile (MeCN), 10 mol% of amino-functionalized ligand, at 75 °C for 2 h.

absence of secondary crystalline phases (Figure 2b). This evidenced the stability of MOF-808 framework under the conditions explored for the post-synthesis modification. Attenuated Total Reflectance - Fourier Transform Infrared (ATR-FTIR) spectra were recorded for the modified MOF-808 materials

(Figure S9). The data shows the appearance of two bands centered at ca. 3450 and 3400 cm⁻¹ associated to the presence of primary amine groups in **MOF-808-4AB** and **MOF-808-5AIP**. Thermogravimetric analyses (TGA) performed on our materials (Figure S8) showed characteristic weight losses corresponding to

the presence of the added ligands and the ultimate material collapse around 350–500 °C, followed by the loss of benzene-1,3,5-tricarboxylic acid (BTC) ligands. The total organic content estimated from TGA curve agree well with the calculated after the above-mentioned ^1H NMR analyses (Table S1).

To assess the accessible porosity of the bifunctional MOF-808 materials, nitrogen adsorption isotherms at 77 K were carried out (Figure 2c). Calculated BET surface areas are collected in Table 1. These experiments showed the expected decreased adsorption capacities after MOF crafting with benzoate ligands, much bulkier in comparison to formates. In particular, the MOFs containing amine groups (**MOF-808-5AIP** and **MOF-808-4AB**) exhibited higher adsorption capacity than those modified with pyridine ligands (**MOF-808-PyDC** and **MOF-808-PyC**), probably due to the lesser extent of the chemical modification (see Table 1). Density Functional Theory (DFT) pore size distribution analyses (Figure 2d) showed the almost disappearance of the adsorption associated to the larger mesopore of original MOF-808 (~2.2 nm) in all cases, indicative of its occupation by benzoate ligands.

2.2. Organocatalytic Activity of Bifunctional MOF-808

In order to evaluate the accessibility and the organocatalytic reactive sites integrated into the MOF-808 framework, bifunctional post-functionalized materials were utilized as heterogeneous catalysts for the Knoevenagel condensation, a widely-used benchmark reaction. The study focused on two distinct parameters while performing the reaction between benzaldehyde and malononitrile: (i) the basicity of the added pyridine and amino groups, and (ii) the potential impact of the pendant carboxylic acid group present in the added functional ligands, which could activate the benzaldehyde before its condensation takes place. The results of the catalytic tests revealed that the MOF-808 materials containing amino groups (**MOF-808-5AIP** and **MOF-808-4AB**) showed higher conversion yields than their equivalents containing pyridine groups (**MOF-808-PyDC** and **MOF-808-PyC**), due to the stronger basic character of the amine group (Table 1). Interestingly, these experiments also evidenced that the materials with dicarboxylic acid ligands (i.e., **MOF-808-5AIP** and **MOF-808-PyDC**) are indeed more active towards Knoevenagel condensations than those containing monocar-

boxylic acid ligands. This evidence suggest that the dicarboxylic acid ligands bind to the $\text{Zr}_6\text{O}_4(\text{OH})_4$ clusters in MOF-808 by only one carboxylate group, with presence of free, pendant carboxylic acid groups in both **MOF-808-5AIP** and **MOF-808-PyDC**. Our hypothesis is that the stabilization of unbound carboxylic acid groups within the MOF-808 plays a role in the reaction mechanism. Specifically, these groups form hydrogen bonds with the benzaldehyde substrate (as illustrated in Computational Modelling section) and create a synergistic effect in conjunction with the amino/pyridine group. This effect boosts the catalytic activity of the final material. **MOF-808-5AIP** showed the best catalytic performance for all materials, displaying full conversion in 2 h at 75 °C. The calculated TON value, normalized to amino-ligand content, is 11.4 at 60 min., which falls within the range of reported Zr-MOFs with structural aminated ligands (Table S2). The heterogeneous nature of the bifunctional organocatalysis in **MOF-808-5AIP** was confirmed through catalyst filtration (Figure S11). To evaluate the stability of the material under reaction conditions, **MOF-808-5AIP** was recycled for subsequent runs. Remarkably, high conversion yields were observed for six consecutive runs (Figure S12), and no loss of crystallinity was observed in PXRD (Figure S1). These findings suggest that **MOF-808-5AIP** holds great potential as a highly active and reusable heterogeneous catalyst for Knoevenagel condensation.

2.3. Suppression of the Bifunctionality in MOF-808-5AIP after Methylation of Pendant Carboxylic Moiety

Based on the catalytic results, it is suggested that the 5AIP ligands are connected to the $\text{Zr}_6\text{O}_4(\text{OH})_4$ clusters in MOF-808 via a single carboxylate group, leaving the other carboxylic group unbound to activate the benzaldehyde. In order to investigate the impact of the available carboxylic acid groups in MOF-808 materials on catalysis, a post-synthetic methylation was carried out on the most active catalyst (**MOF-808-5AIP**) affording a new post-functionalized MOF named **Me-MOF-808-5AIP**. To achieve this objective, a sample of **MOF-808-5AIP** was treated overnight with a typical reagent for the methylation of carboxylic acid, a solution containing trimethylsilyldiazomethane in methanol/toluene (1.5 mL/3.5 mL) at room temperature, leading to the methylation of the unbound carboxylic groups (Figure 3). The

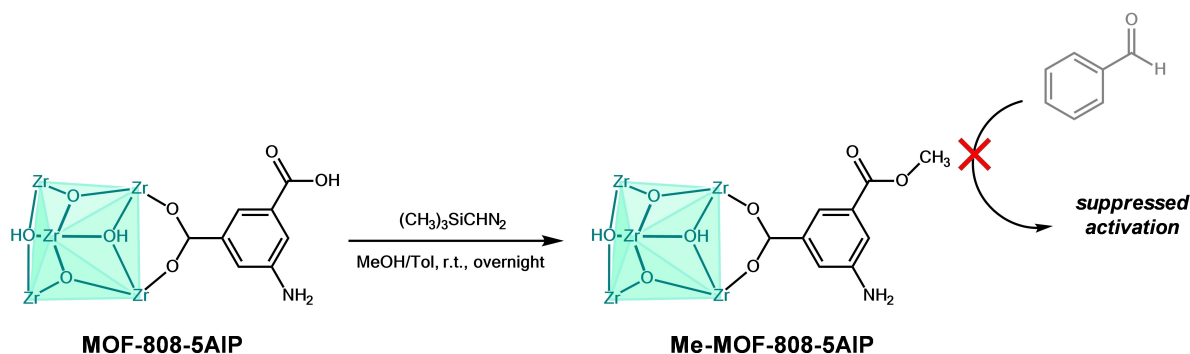


Figure 3. Suppression of the acidic functionality in **MOF-808-5AIP** after methylation of pendant ligand with trimethylsilyldiazomethane.

methyated **Me-MOF-808-5AIP** material was then washed several times with acetone, dried at 60 °C, and digested under acid conditions to perform ^1H NMR characterization. The presence of $-\text{OCH}_3$ groups which are formed through the methylation of free carboxylic groups in the **MOF-808-5AIP** was confirmed, with an observed conversion from acid to ester (singlet at 3.85 ppm in ^1H NMR, Figure S6) of approximately 53% (Table 2). In addition, it was observed that all formate ligands are removed, possibly due to the treatment with methanol,^[14] but the MOF-808 maintained its crystallinity after the reaction with trimethylsilyldiazomethane (Figure S4). The objective of this modification was to investigate whether the transformation of the available carboxylic acid groups into esters would eliminate the bifunctional effects. In fact, the catalytic activity of **Me-MOF-808-5AIP** was significantly decreased under the same conditions, resulting in only 30% yield (Table 2). This provides further evidence for the crucial role of the accessible carboxylic groups in **MOF-808-5AIP** in the catalytic mechanism of Knoevenagel condensation.

2.4. Study on the Spatial Configuration of Carboxylate and Amino Groups

To explore the bifunctional effect between the added organo-catalytic reactive sites in the MOF-808 framework, two additional amino-isophthalic ligands were incorporated through post-synthetic modifications. These ligands, namely 2- and 4-aminoisophthalic acids (2AIP and 4AIP, respectively), have the amino group located at different positions within the ligand structure. In **MOF-808-2AIP**, the amino group is located *ortho* to both carboxylic groups, whereas in **MOF-808-4AIP**, the amino group is located *ortho* and *para* to the different carboxylic groups. The loading of 2AIP and 4AIP was slightly higher than 5AIP in the MOF-808 framework as determined by ^1H NMR (Figure S7, Table 2), and the crystallinity and phase purity was confirmed for the two materials (Figure S3). The MOFs were evaluated for the Knoevenagel condensation between benzaldehyde and malononitrile under the conditions reported above. Remarkably, the relative position of the amino group respect to carboxy group within the AIP ligands incorporated into MOF-808 has a key role to tune the catalytic activity. A significant decrease (20%) and a lack of catalytic activity (0%) for **MOF-808-4AIP** and **MOF-808-2AIP** was observed, respectively (Table 2). These experiments suggested that the spatial arrangement of functional groups (*i.e.*, *meta*

position), prevents unfruitful deactivation of both centers. This allows for simultaneous activation of the reacting substrates.

2.5. Application: Synthesis of Photostabilizers Compounds

The catalytic activity of MOF-808-5AIP was further investigated for various substrates including different aromatic aldehydes and methylene compounds, as shown in Table 3. Compared to the catalytic activity observed when using malononitrile and benzaldehyde as substrates (*i.e.*, 100% in 2 hr at 75 °C), lower yields were determined with ethyl cyanoacetate (*i.e.*, 57% in 24 hr at 90 °C) due to different acidity of these methylene compounds (ethyl cyanoacetate $pK_a = 13.1$, malononitrile $pK_a = 11.1$). To demonstrate the versatility of **MOF-808-5AIP** as heterogeneous catalyst for Knoevenagel condensations, further experiments were carried out by using vanillin or syringaldehyde with ethyl cyanoacetate as substrates to produce ethyl α -cyano-4-hydroxy-3-methoxycinnamate and ethyl 2-cyano-3-(4-hydroxy-3,5-dimethoxyphenyl)-acrylate, respectively. In all cases, conversion yields of 40–50% were achieved after 24 hours of reaction time. These final products are photostabilizers compounds with antioxidant properties commonly used in the formulation of commercial sunscreens. The successful synthesis of a range of final products with valuable applications using **MOF-808-5AIP** as a highly active, reusable heterogeneous catalyst for the Knoevenagel condensation, highlights the potential of bifunctional organocatalytic MOF-808 materials in various fields. These materials offer a promising avenue for the development of efficient and sustainable catalytic systems with a wide range of applications, including in the pharmaceutical, materials, and energy industries. The results of this study pave the way for further investigations into the potential of MOF-808 materials and their derivatives for catalytic applications.

2.6. Acid-base Tandem Organocatalysis by Bifunctional Sites in MOF-808

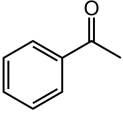
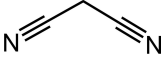
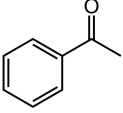
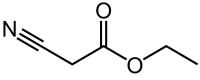
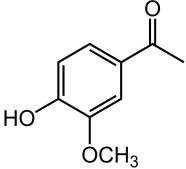
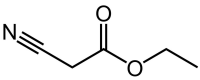
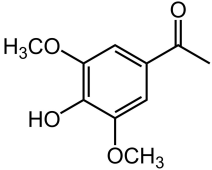
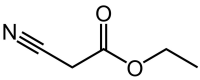
The use of a single solid as catalyst with more than one type of active site to accelerate tandem or cascade reactions is of special interest, resulting in more sustainable and efficient chemical production. Due to the excellent performance of **MOF-808-5AIP** towards Knoevenagel condensation, this material was further evaluated in a tandem reaction that requires

Table 2. Chemical formula and catalytic results for selected materials in the Knoevenagel condensation reaction between benzaldehyde and malononitrile.

Materials	Chemical formula (^1H NMR) ^{a)}	Yield [%] ^{b)}
Me-MOF-808-5AIP	$\text{Zr}_6\text{O}_4(\text{OH})_4(\text{BTC})_2(5\text{AIP})_{0.7}(\text{Me-5AIP})_{0.8}(\text{HCOO})_{1.6}(\text{H}_2\text{O})_{2.9}(\text{OH})_{2.9}$	30
MOF-808-4AIP	$\text{Zr}_6\text{O}_4(\text{OH})_4(\text{BTC})_2(4\text{AIP})_{1.9}(\text{HCOO})_{2.4}(\text{H}_2\text{O})_{1.7}(\text{OH})_{1.7}$	20
MOF-808-2AIP	$\text{Zr}_6\text{O}_4(\text{OH})_4(\text{BTC})_2(2\text{AIP})_{2.2}(\text{HCOO})_{2.2}(\text{H}_2\text{O})_{1.6}(\text{OH})_{1.6}$	0

^{a)} Normalized to 2 BTC. BTC: benzene-1,3,5-tricarboxylate, 5AIP: 5-aminoisophthalate, Me-5AIP: 3-Amino-5-(methoxycarbonyl)benzoate, 4AIP: 4-aminoisophthalate, 2AIP: 2-aminoisophthalate; ^{b)} Reactions conditions: benzaldehyde (0.27 mmol), malononitrile (0.28 mmol), 0.5 mL MeCN ACN, 10 mol% of amino-functionalized ligand, at 75 °C for 2 h.

Table 3. Catalytic activity of MOF-808-5AIP in different basic condensations.^{a)}

Substrate 1	Substrate 2	Temperature [°C]	Time [h]	Yield [%]
		75	2	100
		90	24;48	44;57
		90	24;48	39;72
		90	24	47

^{a)} Reactions conditions: substrate 1 (0.27 mmol), substrate 2 (0.28 mmol), 0.5 mL MeCN ACN and 10 mol% of amine-functionalized ligand.

both the presence of acid and basic sites. In particular, the transformation of benzaldehyde dimethylacetal to benzylidene-malononitrile was evaluated (Figure 4a). The first step (deacetylation) requires an acid catalytic center to hydrolyze benzalde-

hyde dimethylacetal into benzaldehyde. The second step (Knoevenagel condensation) requires basicity, or acid-base functionality (*i.e.*, **MOF-808-5AIP**) to allow the reaction between the benzaldehyde with malononitrile to yield the final product.

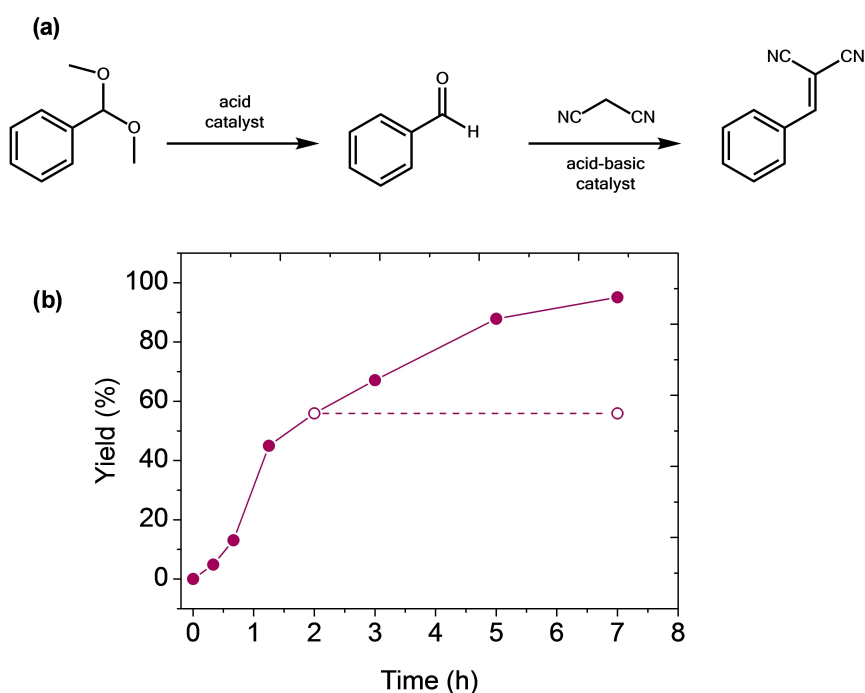


Figure 4. (a) Tandem catalyzed deacetylation-Knoevenagel condensation. (b) Catalytic profile of the tandem deacetalization-Knoevenagel condensation in presence of **MOF-808-5AIP** and heterogeneity test after catalyst filtration (empty circles). Reaction conditions: 10 mol% of amino-functionalised ligands, MeCN ACN, 75 °C.

Under the same reaction conditions used for the Knoevenagel reaction (*i.e.*, 75 °C and 10 mol% of amino-functionalised ligand), a conversion yield of 95% was observed after 7 h of reaction. Hot filtration experiments were performed by filtering off the MOF after 2 h of reaction time (56% conversion), showing a lack of leaching (Figure 4b) and therefore the heterogeneity of the process. The MOF framework is stable after three reaction cycles as determined by PXRD results (Figure S2). Thus, the accessibility of both acid and basic sites within the bifunctional **MOF-808-5AIP** was demonstrated, thereby allowing the bifunctional organocatalytic activity for a benchmark tandem process such as the deacetalization-Knoevenagel condensation.

2.7. Pair Distribution Function Analyses

Pair Distribution Function (PDF) analyses from total X-ray scattering data were carried out to gain structural insight into the molecular interactions within the bifunctional **MOF-808-5AIP** organocatalyst. To assess the structural variations between pristine MOF-808 and the modified material, differential PDF (dPDF) analyses were carried out. Thus, the total PDF signal of pristine MOF-808 was subtracted to that of the modified material, thereby highlighting the structural differences at the local scale between the two materials (Figure 5 and S11). Interestingly, dPDF signal for **MOF-808-5AIP** show features between ~2.4–2.7 Å, that suggest the occurrence of hydrogen bonding of different strength between the free carboxylic acid groups in the framework and physisorbed water molecules. Furthermore, the distinctive signals centered at ~3.3 and 3.7 Å are identified, which can be explained by a local distortion of the $\text{Zr}_6\text{O}_4(\text{OH})_4$ clusters^[15] caused by the partial replacement of formic acid by 5AIP ligands. A close inspection of the data also revealed the appearance of new Zr(IV)-OH distances after the

modification with 5AIP ligands, which suggests the partial activation of the cluster and subsequent deprotonation of the aqua ligands and protonation of the amino groups.

2.8. Computational Modelling

To gain further insights into the catalytic mechanism of **MOF-808-5AIP**, a theoretical mechanistic investigation was carried out on the Knoevenagel condensation reaction involving benzaldehyde and malononitrile substrates. The MOF chosen for the study was the one that showed the highest catalytic activity, and therefore the structure of the $[\text{Zr}_6(\text{CH}_3\text{COO})_6(\text{HCOO})_4(\text{OH})_4\text{O}_4(5\text{AIP})_2]$ model cluster was analyzed, with particular attention paid to the positioning of 5-aminoisophthalic acid in close proximity. This initial geometry enables interactions between the pendant acid and basic sites of the two AIP ligands and also possess the higher thermodynamic stability among all calculated initial structures (see SI for details). In the model cluster, we selected the structure containing benzaldehyde and malononitrile substrates situated near 5AIP ligands as the initial reagent system (**R** in Figure 6). Comparison of the energy of the initial complex **R**, including the substrates and that of the cluster and substrates calculated separately, allowed us to estimate an energy of interaction Cluster-Substrates of approximately 15 kcal/mol. The main contribution to the interaction energy is attributed to two hydrogen bonding interactions: a) $\text{O}-\text{H}\cdots\text{O}=\text{C}$ between carboxylic group of 5AIP ligand and benzaldehyde and b) $\text{C}-\text{H}\cdots\text{NH}_2-\text{C}$ between amine group of L ligand and CH in malononitrile substrate (see in **R** structure of Figure 6).

Exploration of the potential energy surface indicated that the overall reaction follows a two-step pathway. The first step involves the deprotonation of the malononitrile by the amine fragment of the bifunctional organocatalytic ligand. Direct

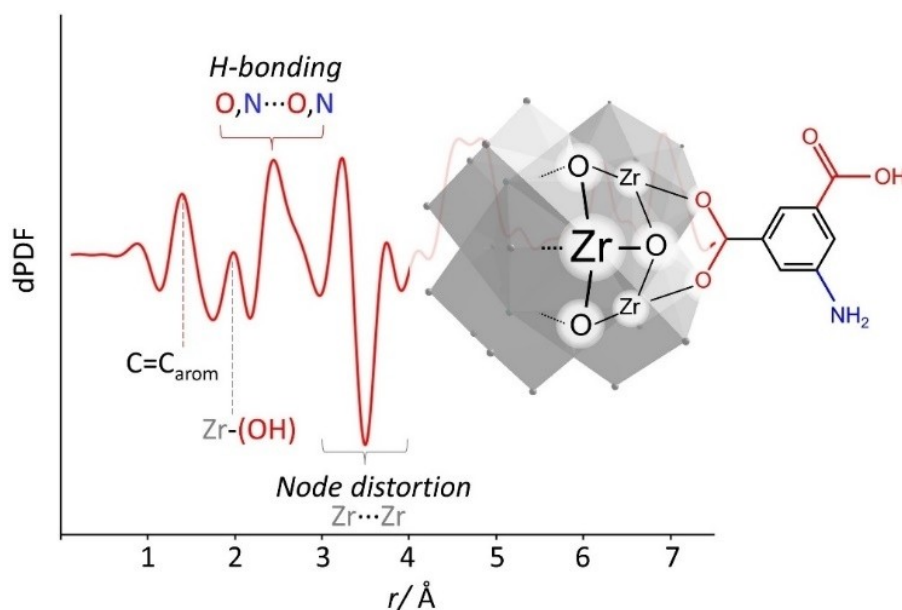


Figure 5. Differential PDF corresponding to the new atom – atom distances formed upon modification of the MOF-808 framework with 5AIP ligands.

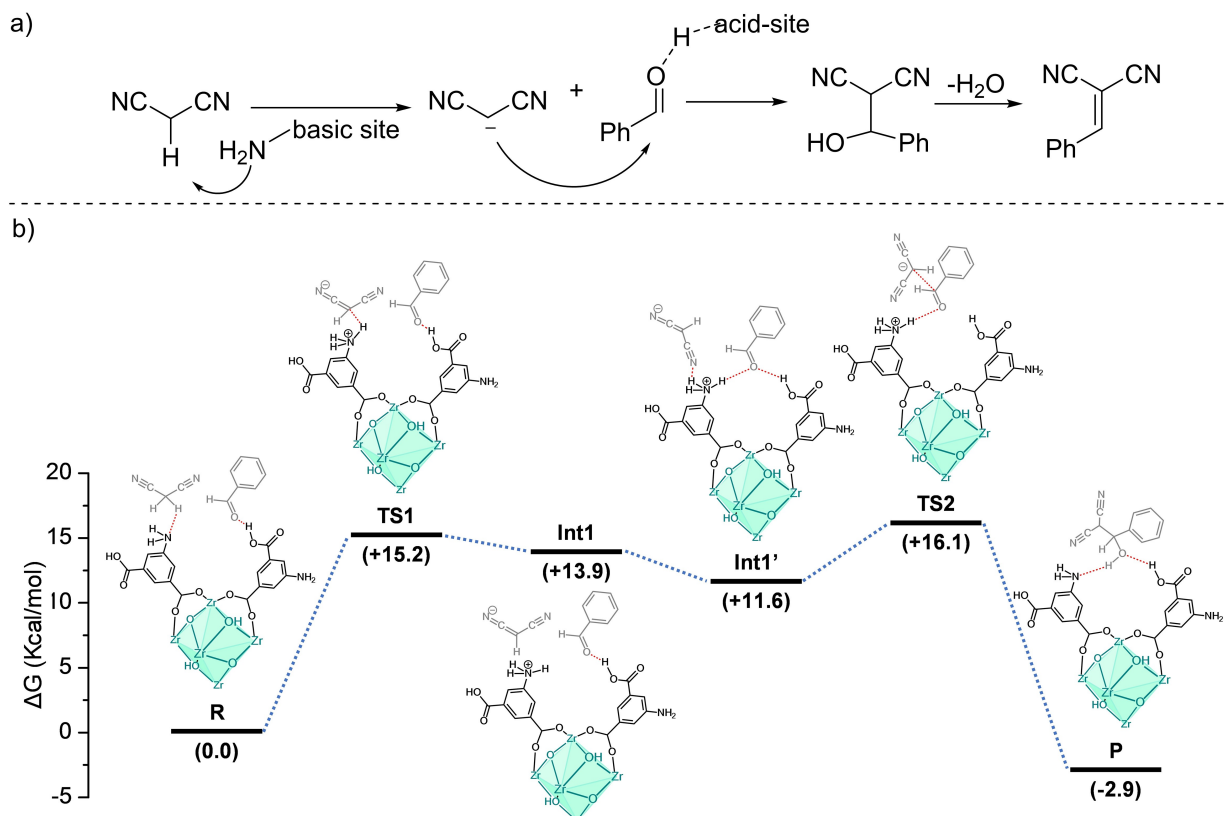


Figure 6. a) Scheme of the bifunctional material and the Knoevenagel reaction. b) Energy profile found in the study of the catalytic mechanism of the reaction between benzaldehyde and malononitrile in the presence of the model cluster. Electronic energy values are shown in Kcal/mol. Precise models can be found in the Supporting Information (section S9).

deprotonation of malononitrile in **R** produces the intermediate 1 (**Int1** in Figure 6) through an endergonic reaction (by approximately 14 kcal/mol) with a kinetic barrier of around 15 kcal/mol. These results suggest that the acid-base equilibrium is significantly shifted towards the protonated malononitrile. The reaction can proceed only when the deprotonation event occurs in close proximity to the benzaldehyde. Such proximity is achieved in **Int1'**, which is accessible from a nearly barrierless rearrangement from **Int1** that results in an extra stabilization of approximately 2 kcal/mol. The substrates in **Int1'** are fixed together by several hydrogen bonds, including N–H...N≡C bonding between the deprotonated malononitrile and protonated amino group, as well as O–H...O=C and N–H...O=C bonding between the benzaldehyde and the carboxylic fragment or protonated amino group of the **L** ligand. This intermediate structure has a predetermined geometry that facilitates the formation of C–C bonds.

With the system appropriately oriented, the C–C bond formation occurs through a low kinetic barrier. This process is coupled to the simultaneous proton transfer from the amine nitrogen to the oxygen atom in the product. The transition state found (**TS2**) is just 4.5 kcal/mol above the intermediate structure **Int1'**. Structure of **TS2** is mainly related to C–C bond formation, while the amine group is still protonated. Subsequently, a barrierless proton transfer from the amine group to the alkoxide (which is produced as a result of C–C bond

formation) takes place consecutively, leading to the formation of the final reaction product, **P**. Overall, the reaction from **R** to **P** is slightly exothermic by approximately 3 kcal/mol.

The basic reactivity of the Knoevenagel reaction is summarized in Figure 6a, illustrating the roles of both the basic site and the acid sites in obtaining the final product. The overall profile shown in Figure 6b indicates that the rate-limiting step in the process is the deprotonation of malononitrile. Since the process is reversible, the malononitrile is likely to undergo reverse re-protonation after being deprotonated, unless the electrophilic benzaldehyde is in close proximity. Thus, it seems that the bifunctional design of the organocatalytic system lays in the co-existence of the amine group (able to abstract a proton from malononitrile) with the acidic group in the correct disposition to fix the electrophile in the appropriate orientation relative to the nucleophile. Such arrangement offers an alternative pathway to the re-protonation of malonitrile. Accordingly, experimental results using the ester containing organocatalytic **L'** ligand (**L'** = C₆H₃(COO)(NH₂)(COOCH₃) in **Me-MOF-808-5AIP** suggest that methylation of acid fragment has a detrimental effect in the catalytic output. Thus, theoretical results suggest that the main role of carboxylic acid is not related to its possible behavior as acidic catalytic site. Otherwise, the importance of carboxylic groups is primarily understood as an entropic effect, owing its ability to pre-organize the substrates in such a way

that the generation of the final product is favored over unproductive processes such as re-protonation of malonitrile.

3. Conclusions

In this work, we have synthesized a series of post-synthetically functionalized MOF-808 catalysts incorporating both carboxylic and nitrogen moieties in a single pendant ligand. Our results demonstrate an improved catalytic effect for bifunctional materials, with **MOF-808-5AIP** showing particularly promising activity for Knoevenagel and deacetylation-Knoevenagel tandem condensation reactions. This material exhibited both high activity and remarkable stability across multiple catalytic cycles, owing to the close proximity of the active functional groups. Importantly, our computational studies revealed that the spatial arrangement of the moieties, specifically in the metha position, played a critical role in the reaction mechanism. These findings underscore the potential of precisely tailored MOF-based platforms for the development of advanced, biomimetic organo-catalysts with high activity and stability.

Supporting Information

Supporting Information (SI) is available from the Wiley Online Library or from the author. SI includes syntheses details, powder X-ray diffraction, ¹H Nuclear Magnetic Resonance (¹H NMR) Spectroscopy, Thermogravimetric Analyses (TGA), Attenuated total reflectance - Fourier Transform Infrared Spectroscopy (ATR-FTIR), Pair Distribution Function (PDF) analyses, catalytic studies, and computational modelling. The authors have cited additional references within the Supporting Information.^[16–25]

Acknowledgements

We thank the Spanish Ministry of Science and Innovation MCIN/AEI/10.13039/501100011033 (grants No. PID2021-123839OB-I00, RYC2018-024328-I, CEX2018-000805-M, PID2021-122299NB-I00, TED2021-130470B-I00, TED2021-129999B-C32) and the “European Union NextGenerationEU/PRTR” (grant No. EUR2020-112294) and ‘Comunidad de Madrid’, European Structural Funds (S2018/NMT-4367), proyectos sinérgicos I+D (Y2020/NMT6469) and Comunidad Autónoma de Madrid (SI1/PJ1/2019-00237). Part of this research was carried out at P02.1 beamline at DESY, a member of the Helmholtz Association (HGF). We acknowledge DESY (Hamburg, Germany), a member of the Helmholtz Association HGF, for the provision of experimental facilities. Beamtime was allocated for proposal I-20211230 EC.

Conflict of Interests

The authors declare no conflict of interest.

Data Availability Statement

The data that support the findings of this study are available in the supplementary material of this article.

Keywords: Metal-organic framework · MOF-808 · bifunctional organocatalysis · Knoevenagel condensation · pair distribution function · computational modelling

- [1] J. N. Appaturi, R. Ratti, B. L. Phoon, S. M. Batagarawa, I. U. Din, M. Selvaraj, R. J. Ramalingam, *Dalton Trans.* **2021**, 50, 4445–4469.
- [2] a) R. Freund, S. Canossa, S. M. Cohen, W. Yan, H. Deng, V. Guillerme, M. Eddaoudi, D. G. Madden, D. Fairen-Jimenez, H. Lyu, L. K. Macreadie, Z. Ji, Y. Zhang, B. Wang, F. Haase, C. Wöll, O. Zaremba, J. Andreato, S. Wuttke, C. S. Diercks, *Angew. Chem. Int. Ed.* **2021**, 60, 23946–23974; b) G. Maurin, C. Serre, A. Cooper, G. Férey, *Chem. Soc. Rev.* **2017**, 46, 3104–3107; c) H.-C. Zhou, J. R. Long, O. M. Yaghi, *Chem. Rev.* **2012**, 112, 673–674.
- [3] a) K. Hemmer, M. Cokoja, R. A. Fischer, *ChemCatChem.* **2021**, 13, 1683–1691; b) J. Liu, T. A. Goetjen, Q. Wang, J. G. Knapp, M. C. Wasson, Y. Yang, Z. H. Syed, M. Delferro, J. M. Notestein, O. K. Farha, J. T. Hupp, *Chem. Soc. Rev.* **2022**, 51, 1045–1097.
- [4] a) A. Bavykina, N. Kolobov, I. S. Khan, J. A. Bau, A. Ramirez, J. Gascon, *Chem. Rev.* **2020**, 120, 8468–8535; b) C.-D. Wu, M. Zhao, *Adv. Mater.* **2017**, 29, 1605446.
- [5] O. Karagiari, W. Bury, J. E. Mondloch, J. T. Hupp, O. K. Farha, *Angew. Chem. Int. Ed.* **2014**, 53, 4530–4540.
- [6] a) S. Rojas-Buzo, P. García-García, A. Corma, *Green Chem.* **2018**, 20, 3081–3091; b) R. R. Prasad, D. M. Dawson, P. A. Cox, S. E. Ashbrook, P. A. Wright, M. L. Clarke, *Chem. Eur. J.* **2018**, 24, 15309–15318.
- [7] a) Y.-B. Huang, J. Liang, X.-S. Wang, R. Cao, *Chem. Soc. Rev.* **2017**, 46, 126–157; b) A. Dhakshinamoorthy, H. Garcia, *ChemSusChem.* **2014**, 7, 2392–2410.
- [8] a) H. Liu, F.-G. Xi, W. Sun, N.-N. Yang, E.-Q. Gao, *Inorg. Chem.* **2016**, 55, 5753–5755; b) S. A. A. Razavi, A. Morsali, *Inorg. Chem.* **2019**, 58, 14429–14439; c) R. Srirambalaji, S. Hong, R. Natarajan, M. Yoon, R. Hota, Y. Kim, Y. H. Ko, K. Kim, *Chem. Commun.* **2012**, 48, 11650–11652; d) H. He, F. Sun, B. Aguila, J. A. Perman, S. Ma, G. Zhu, *J. Mater. Chem. A* **2016**, 4, 15240–15246; e) Y. Zhang, Y. Wang, L. Liu, N. Wei, M.-L. Gao, D. Zhao, Z.-B. Han, *Inorg. Chem.* **2018**, 57, 2193–2198; f) Y. Hu, J. Zhang, H. Huo, Z. Wang, X. Xu, Y. Yang, K. Lin, R. Fan, *Catal. Sci. Technol.* **2020**, 10, 315–322; g) B. Li, Y. Zhang, D. Ma, L. Li, G. Li, G. Li, Z. Shi, S. Feng, *Chem. Commun.* **2012**, 48, 6151–6153; h) M. Yang, Y.-S. Bao, M.-L. Zhou, S. Wang, Y.-H. Cui, W. Liu, L.-C. Li, L.-X. Meng, Y.-Y. Zhang, Z.-B. Han, *Catal. Lett.* **2023**; i) M. Qin, J. Gao, D. Wei, L. Li, C. Li, L. Yang, *J. Inorg. Organomet. Polym.* **2022**, 32, 37–46.
- [9] a) F. Ghobakhloo, D. Azarifar, M. Mohammadi, H. Keypour, H. Zeynali, *Inorg. Chem.* **2022**, 61, 4825–4841; b) F.-G. Xi, H. Liu, N.-N. Yang, E.-Q. Gao, *Inorg. Chem.* **2016**, 55, 4701–4703; c) Y. Yang, H.-F. Yao, F.-G. Xi, E.-Q. Gao, *J. Mol. Catal. A* **2014**, 390, 198–205.
- [10] a) H. Furukawa, F. Gándara, Y.-B. Zhang, J. Jiang, W. L. Queen, M. R. Hudson, O. M. Yaghi, *J. Am. Chem. Soc.* **2014**, 136, 4369–4381; b) J. Jiang, F. Gándara, Y.-B. Zhang, K. Na, O. M. Yaghi, W. G. Klemperer, *J. Am. Chem. Soc.* **2014**, 136, 12844–12847.
- [11] a) X. Meng, H.-N. Wang, L.-S. Wang, Y.-H. Zou, Z.-Y. Zhou, *CrystEngComm.* **2019**, 21, 3146–3150; b) H. Dong, G.-X. Yang, X. Zhang, X.-B. Meng, J.-L. Sheng, X.-J. Sun, Y.-J. Feng, F.-M. Zhang, *Chem. Eur. J.* **2018**, 24, 17148–17154; c) K. H. Cho, S. K. Chitale, S.-J. Kim, G.-Y. Cha, D.-Y. Hong, S. G. Ryu, J.-S. Chang, Y. K. Hwang, *Microporous Mesoporous Mater.* **2019**, 285, 61–69.
- [12] X. Wang, Z. Xu, L. Li, Y. Zhao, R. Su, G. Liang, B. Yang, Y. Miao, W. Meng, Z. Luan, K. Li, H. Xi, R. Zou, *ACS Appl. Nano Mater.* **2020**, 3, 11442–11454.
- [13] a) H.-H. Mautschke, F. Drache, I. Senkova, S. Kaskel, F. X. L. i Xamena, *Catal. Sci. Technol.* **2018**, 8, 3610–3616; b) K. D. Nguyen, N. T. Vo, K. T. M. Le, K. V. Ho, N. T. S. Phan, P. H. Ho, H. V. Le, *New J. Chem.* **2023**, 47, 6433–6447.
- [14] a) I. Romero-Muñiz, C. Romero-Muñiz, I. del Castillo-Velilla, C. Marini, S. Calero, F. Zamora, A. E. Platero-Prats, *ACS Appl. Mater. Interfaces.* **2022**, 14, 27040–27047; b) C. Jia, F. G. Cirujano, B. Bueken, B. Claes, D. Jonckheere, K. M. Van Geem, D. De Vos, *ChemSusChem.* **2019**, 12, 1256–1266.

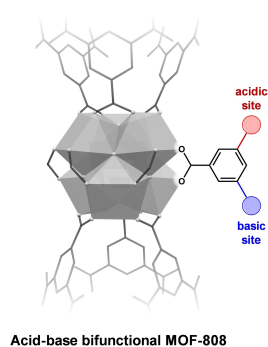
- [15] A. E. Platero-Prats, A. Mavrandonakis, L. C. Gallington, Y. Liu, J. T. Hupp, O. K. Farha, C. J. Cramer, K. W. Chapman, *J. Am. Chem. Soc.* **2016**, *138*, 4178–4185.
- [16] M. Basham, J. Filik, M. T. Wharmby, P. C. Y. Chang, B. el Kassaby, M. Gerring, J. Aishima, K. Levik, B. C. A. Pulford, I. Sikharulidze, D. Sneddon, M. Webber, S. S. Dhesi, F. Maccherozzi, O. Svensson, S. Brockhauser, G. Náray, A. W. Ashton, *J. Synchrotron Radiat.* **2015**, *22*, 853–858.
- [17] P. Juhás, T. Davis, C. L. Farrow, S. J. L. Billinge, *J. Appl. Crystallogr.* **2013**, *46*, 560–566.
- [18] a) C. J. Cramer, D. G. Truhlar, *Phys. Chem. Chem. Phys.* **2009**, *11*, 10757; b) Y. Zhao, D. G. Truhlar, *Theor. Chem. Acc.* **2008**, *120*, 215.
- [19] S. E. Wheeler, K. N. Houk, *J. Chem. Theory Comput.* **2010**, *6*, 395.
- [20] M. J. Frisch, G. W. Trucks, H. B. Schlegel, G. E. Scuseria, M. A. Robb, J. R. Cheeseman, G. Scalmani, V. Barone, B. Mennucci, G. A. Petersson, H. Nakatsuji, M. Caricato, X. Li, H. P. Hratchian, A. F. Izmaylov, J. Bloino, G. Zheng, J. L. Sonnenberg, M. Hada, M. Ehara, K. Toyota, R. Fukuda, J. Hasegawa, M. Ishida, T. Nakajima, Y. Honda, O. Kitao, H. Nakai, T. Vreven, J. A. Montgomery, Jr., J. E. Peralta, F. Ogliaro, M. Bearpark, J. J. Heyd, E. Brothers, K. N. Kudin, V. N. Staroverov, R. Kobayashi, J. Normand, K. Raghavachari, A. Rendell, J. C. Burant, S. S. Iyengar, J. Tomasi, M. Cossi, N. Rega, J. M. Millam, M. Klene, J. E. Knox, J. B. Cross, V. Bakken, C. Adamo, J. Jaramillo, R. Gomperts, R. E. Stratmann, O. Yazyev, A. J. Austin, R. Cammi, C. Pomelli, J. W. Ochterski, R. L. Martin, K. Morokuma, V. G. Zakrzewski, G. A. Voth, P. Salvador, J. J. Dannenberg, S. Dapprich, A. D. Daniels, Ö. Farkas, J. B. Foresman, J. V. Ortiz, J. Cioslowski, D. J. Fox D. J. *Gaussian 09 (Revision D.01)*, Gaussian, Inc., Wallingford CT, **2011**.
- [21] a) Y. Zhao, D. G. Truhlar, *Acc. Chem. Res.* **2008**, *41*, 157; b) Y. Zhao, D. G. Truhlar, *Chem. Phys. Lett.* **2011**, *502*, 1.
- [22] D. Andrae, U. Haeussermann, M. Dolg, H. Stoll, H. Preuss, *Theor. Chim. Acta.* **1990**, *77*, 123.
- [23] A. W. Ehlers, M. Bohme, S. Dapprich, A. Gobbi, A. Hollwarth, V. Jonas, K. F. Kohler, R. Stegmann, A. Veldkamp, G. Frenking, *Chem. Phys. Lett.* **1993**, *208*, 111.
- [24] a) W. J. Hehre, R. Ditchfield, J. A. People, *J. Chem. Phys.* **1972**, *56*, 2257; b) M. Francl, W. J. Pietro, W. J. Hehre, J. S. Binkley, M. S. Gordon, D. J. DeFrees, J. A. Pople, *J. Chem. Phys.* **1982**, *77*, 3654.
- [25] A. V. Marenich, C. J. Cramer, D. G. Truhlar, *J. Phys. Chem. B.* **2009**, *113*, 6378–6396.

Manuscript received: April 12, 2024

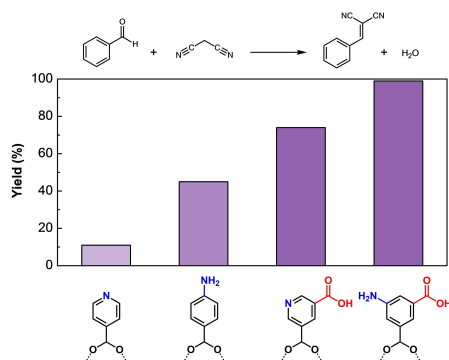
Revised manuscript received: May 14, 2024

Accepted manuscript online: May 31, 2024

Version of record online: ■■, ■■



The introduction of an acidic and a basic functionality, precisely located, within a metal-organic framework (MOF) enhances the catalytic activity



for Knoevenagel and related condensations. Modified MOF-808 containing 5-aminoisophthalic yielded higher rates among all explored materials.

J. M. Moreno, R. Gil-San-Millan, R. Mas-Ballesté, J. Alemán*, A. E. Platero-Prats*

1 – 11

Enhanced Organocatalytic Processes through an Engineered Acid-Base Site Bifunctional Pore in a Zirconium Metal-Organic Framework

